Determination of void fraction in wet-gas vertical flows via differential pressure measurement

Determination of Void Fraction in Wet-Gas Vertical Flows via Differential Pressure Measurement

Names of Authors: Paul Tait[a], Yuan Chen[a], Wataru Senjyu[b], Toru Watanabe[b], Yasuo Inamura[b], Valentina Presotto[c], Radek Mojsak[c], Gabriele Chinello[d], Jiabin Jia[a]

Affiliation: The University of Edinburgh[a], Fuji Electric Co[b], Spirax Sarco Ltd[c], TUV-SUD National Engineering Laboratory[d]

Author Contributions

Paul Tait: Writing – Original draft, Formal analysis, investigation, methodology
Yuan Chen: Writing – Review & editing; Formal analysis
Wataru Senjyu: Conceptualization, Resources
Toru Watanabe: Resources
Yasuo Inamura: Resources
Valentina Presotto: Investigation, Conceptualization
Radek Mojsak: Resources, Conceptualization
Gabriele Chinello: Investigation, Conceptualization, Writing – Review & editing
Jiabin Jia: Conceptualization, Supervision, Project Administration, Writing – Review & editing, Funding Acquisition

Corresponding author's contact details: jiabin.jia@ed.ac.uk; +44(0)131 651 3568

Abstract

The measurement of void fraction in multiphase flow is important for a wide range of industrial processes. Existing methods for void fraction measurement require intrusive, expensive and potentially hazardous equipments which constrict the flow, adding both capital and operational costs. Two phase flow experiments were carried out at the National Engineering Laboratory (NEL) to measure void fraction via pressure drop in a vertical pipe. Additional experiments are carried out at Spirax Sarco Inc. to validate the efficacy of the method on steam/water flow mixtures at high temperature and pressure, in gas mass fraction range between 0.17 and 0.95 and void fraction range between 0.75 and 1.0. The void fraction calculated by the presented differential pressure (dP) method is confirmed via established correlations. The work demonstrates the efficacy of a low cost, non-intrusive method to determine void fraction in two phase flow over a wide range of flow conditions.

Keywords:

Void Fraction
Multiphase Flow
Differential Pressure
Steam
Geothermal

1. Introduction

The measurement of void fraction in multiphase flow is important for a wide range of industrial processes, including the extraction and transportation of natural gas in which the flow is composed of a mixture of condensed hydrocarbons, water and gas, and in the production of steam in the power generation sector, in which the flow is composed of a saturated steam and water mixture. Accurate, rapid on-line measurement of two-phase flow is critical to provide process operators with real-time information about flow conditions so that the process parameters can be adjusted, if necessary, to maintain production efficiency. These measurements can also provide real-time information which may indicate faults which require attention. A relevant example of this is in the transportation of CO_2 to the injection site in the carbon capture and storage (CCS) process, in which a rapid increase in void fraction would indicate a failure in the compression train which is used to condense captured CO_2 into the liquid phase.

The ideal multiphase flow metering system should be accurate, robust enough to withstand test conditions, require little calibration or maintenance work (as they are often located in harsh environments), affordable, and

able to continuously monitor flow conditions [1]. A wide range of methods for the measurement of two-phase flows have been proposed in the past 60 years.

Electrical resistance tomography, electrical capacitance tomography and wire mesh sensors have been used to accurately measure void fraction in oil-water [2] and air-water [3] systems but these are not accurate for flow conditions in which the gas phase dominates in terms of volume fraction. Ultrasonic meters have been used in some circumstances to measure void fraction [4, 5] but are expensive when applied to larger pipe diameters and are mostly applicable to bubble flow conditions. Quick-closing valves can be used to determine the average void fraction across a section of pipe, but as they interrupt the process flow, these are normally used to calibrate non-intrusive methods [6]. Radiative methods such as gamma ray [7], X-ray [8] and neutron scattering [9] are non-intrusive and can provide spatial resolution, but are high in cost and potentially dangerous, requiring additional safety precautions and protections to be installed to minimise exposure to harmful radiation.

This paper continues the development of a method proposed by Jia et al. [10] which has the potential to provide online, non-invasive, continuous measurements of gas void fraction for two-phase flows with low capital cost and maintenance requirements. Further investigation of the differential pressure (dP) method has been carried out by Gui et al. [11], who carried out measurements in steam-water bubble flow for comparison with optical and radiative methods at conditions similar to those in the steam generator of a nuclear power plant. The dP method is found to be accurate to within 15% of expected values. Additional work has been carried out on bubble reactors by Hernandez-Alvarado et al. [12], in which the dP method is found to match gamma densitometry measurements to within 10%, to evaluate the frequency of slugs in pipe [13] and to validate models of pressure drop prediction in conjunction with conductive methods [14]. However, there currently exists no study of this method in large circular pipes up to 4" in diameter, with flows with high void fractions in the annular and annular mist regions.

This approach can complement existing flow measurement methods to provide a more comprehensive understanding of flow conditions within vertical pipe sections without the need for further invasive or expensive apparatus. The method uses a model derived from Bernoulli's principle of energy conservation to determine void fraction using simple differential pressure measurements in a vertical pipe.

In previous work [10], the validity of the model is evaluated using an air-water system with void fractions from 0 to 0.5, and Reynolds numbers lower than 100,000. In this work, the validity of the model is evaluated via experimental testing at gas void fractions higher than 0.5 and at Reynolds numbers from 525,000 to 2,921,000 in the wet-gas high-pressure facility of TUV-SUD National Engineering Laboratory. A second set of tests is carried out in the wet-steam facility of Spirax Sarco to assess the potential of the differential pressure method for flow conditions and temperatures typical of commercial steam flow applications, which demonstrates its potential for use in industrial or power generation scenarios with medium to high-quality steam. Gas void fractions up to 0.99 are tested. This approach has the potential to form the basis of a low-cost, accurate, continuous online void fraction measurement method for multiphase flows over a wide range of flow conditions.

2. Measurement of Void Fraction via Differential Pressure Method

2.1 Derivation of Equations

The proposed differential pressure model is based on Bernoulli's principle of energy conservation within a flow conduit, i.e. that in a steady flow in a streamline, the sum of all forms of energy is the same at all points. This can be described mathematically by:

$$\frac{1}{2}\rho v^2 + \rho g h + P = constant \tag{1}$$

where $\frac{1}{2}\rho v^2$ is kinetic energy, $\rho g h$ is potential energy and P is pressure. In the case of a vertical tube through which a two-phase mixture is flowing, with tapping points located at h_1 and h_2, the expression can be expanded as:

$$\frac{1}{2}\rho_m v_1^2 + \rho_m g h_1 + P_1 = \frac{1}{2}\rho_m v_2^2 + \rho_m g h_2 + P_2 + F_p \tag{2}$$

where ρ_m is the average density of the fluid mixture, subscripts 1 and 2 refer to tapping point locations 1 and 2, and F_p is the pressure drop between the two points due to frictional effects. If the pipe is of constant cross-

sectional area, and we assume that any difference in flow velocity between the two points is negligible, the approximation $v_1 = v_2$ and cancel out the kinetic energy from each side, simplifying the expression to:

$$\rho_m g h_1 + P_1 = \rho_m g h_2 + P_2 + F_p \tag{3}$$

If location 1 is taken as a reference for which $h_1 = 0$, and the location of point 2 is taken to be at height $h_2 = 0 + h$, it can be further simplified as follows:

$$P_1 = \rho_m g h + P_2 + F_p \tag{4}$$

$$P_1 - P_2 = \Delta P = \rho_m g h + F_p \tag{5}$$

The two-phase flow density can be calculated using the gas void fraction (α_g) and the individual densities of the two flow components. This is substituted into equation (7) and rearranged to solve for the gas void fraction.

$$\rho_m = (1 - \alpha_g)\rho_l + \alpha_g \rho_g \tag{6}$$

$$\Delta P = \left[(1 - \alpha_g)\rho_l + \alpha_g \rho_g\right] g h + F_p \tag{7}$$

$$\alpha_g = \frac{\Delta P - \rho_l g h - F_p}{(\rho_g - \rho_l) g h} \tag{8}$$

In Jia et al. (2015) the flow is dominated by the liquid phase. This allows the gas density to be approximated to 0, simplifying the final expression for gas void fraction. For the test conditions described in this work, the flow is dominated in terms of volume by the gas phase, so new expressions for the friction factor and void fraction must be found. The expression for void fraction is derived from equation (8).

$$\alpha_g = \frac{\Delta P}{(\rho_g - \rho_l) g h} - \frac{\rho_l}{(\rho_g - \rho_l)} - \frac{F_p}{(\rho_g - \rho_l) g h} \tag{9}$$

The frictional pressure drop F_p can be calculated via equation (11). The Fanning friction factor C_f for Reynolds numbers between 2100 and 10^5, is calculated with equation (12) [15], while equation (13) is used for Reynolds numbers greater than 10^4 [16]. There is some overlap between expressions where the Reynolds number is between 10^4 and 10^5, in these cases equation (13) is used for consistency with the majority of flow conditions tested in this work, which have Re > 10^5. The term v_m is the mean velocity of the two-phase flow with the assumption of no-slip conditions and is defined by equation (10), in which A is the pipe cross-sectional area. Average flow viscosity in equation (14) is calculated using the method of Dukler et al. [17].

$$v_m = \frac{m_g}{A \rho_g} + \frac{m_l}{A \rho_l} \tag{10}$$

$$F_p = \frac{2 C_f \rho_m h v_m^2}{D} \tag{11}$$

$$C_f = \frac{0.0791}{Re^{0.25}} \tag{12}$$

$$C_f = 0.0014 + \frac{0.125}{Re^{0.32}} \tag{13}$$

$$Re = \frac{\rho_m v_m D}{\mu_m} \tag{14}$$

Substituting equation (11) into equation (9) yields the new expression for gas void fraction.

$$\alpha_g = \frac{\Delta P}{(\rho_g - \rho_l) g h} - \frac{\rho_l}{(\rho_g - \rho_l)} - \frac{2 C_f \rho_m v_m^2}{(\rho_g - \rho_l) g D} \tag{15}$$

The first two terms of equation (15) refer to the contribution from static head, which can be measured using a simple dP measurement. The third term refers to the contribution from frictional effects. For flow situations in which the contribution to overall void fraction from friction is small in comparison to those from static head, the void fraction can be approximated as follows:

$$\alpha_g \cong \frac{\Delta P}{(\rho_g - \rho_l) g h} - \frac{\rho_l}{(\rho_g - \rho_l)} \tag{16}$$

2.2 Model Assumptions

Equation (15) assumes homogeneous, isothermal flow, no-slip condition at the pipe wall, and equal velocities at upstream and downstream sections. Equation (16) makes the additional assumption that contribution to the void fraction from frictional pressure loss is negligible in comparison to the static component, and may be useful in cases where there is no method to measure individual mass flow rates of gas and liquid or mean flow superficial velocity. It can also be reasonably assumed that the gas compressibility is low as the overall pressure

of the flow system is high, and that over the short measurement length between differential pressure tapping points, the pressure gradient is constant.

Both equations are also based on the assumption of a constant two-phase flow density (equation (6)) which does not apply to the churn, slug, or bubble flow regime. However, measurements are made over a length of pipe between two differential pressure sensors recording data at a rate of at least 1 Hz for 120 seconds. This allows the mean density to be approximated over space and time, and the model is used to determine the mean local void fraction for the time interval over which measurements are made for this pipe section. The performance of the model using both equations (15) and (16) are presented in Section 5.

3. Experimental Setup and Procedures

Experiments were carried out at two separate test locations. Tests with a mixture of nitrogen and water were carried out at TUV-SUD National Engineering Laboratory (NEL) high-pressure gas facility, based in East Kilbride, UK. Tests with steam/water flows were carried out at the Spirax Sarco Technology Centre in Cheltenham, UK. In both cases, differential pressure across a 500 mm section of vertical pipe were measured. This 500 mm section is located at least 10 times pipe diameter downstream of a 90° bend or a blind tee to allow the flow to fully develop.

Differential pressure is recorded using a Yokogawa EJX110A differential pressure sensor with measurement range 0.1 - 5 kPa, which is connected to the test section via ¾" flanges. OPTIMUS series diaphragm sealed flange connections from PCI Instruments, with EJXC80A silicon oil-filled impulse lines were used to connect the differential pressure sensor to the pressure tapping points and ensure measurement accuracy. At both test facilities, absolute pressure and temperature measurements are recorded just before the 500 mm test section. Prior to each test set, the zero point of the Yokogawa differential pressure sensor is adjusted at atmospheric pressure and no flow, if necessary.

In each test, after stable flow conditions are reached, all temperature, pressure and flow data are simultaneously recorded at a sampling rate of at least 1 Hz for 120 seconds using proprietary software available at the test site. The average differential pressure reading across the test section is used to calculate the void fraction as described in Section 2.

3.1 TUV-SUD NEL test description

The NEL high-pressure wet-gas flow rig can provide two-phase flow of nitrogen and water at pressures from 10 to 63 bar_g and temperature of 20 $\pm$ 0.3 ^oC. The test section area can accommodate horizontal and vertical sections of pipe up to 12 m in length and 4 m in height. A diagram of the test rig is shown in Figure 1.

In this test campaign a vertical section is added to the test section area, as shown in Figure 2. The direction of flow is from left to right. The location of the differential pressure sensor on the vertical pipe section is shown on Figure 2, along with its two tapping points. Temperature and absolute pressure measurements are made along the length of both the vertical and horizontal parts of the test section.

Individual flowrates of nitrogen gas and liquid water at each test condition are obtained using the test rig's ultrasonic and Coriolis reference flow meters respectively, prior to the two flow streams being mixed. The rig's reference flowmeters are traceable to national and international standards. The measurement uncertainty for individual gas and liquid flow measurements prior to mixing are $\pm$ 0.35% for gas and $\pm$ 0.5% for liquid at 95% confidence level. The vertical pipe section is constructed from 4" NPS carbon steel with inner diameter 3.826" (97.18 mm).

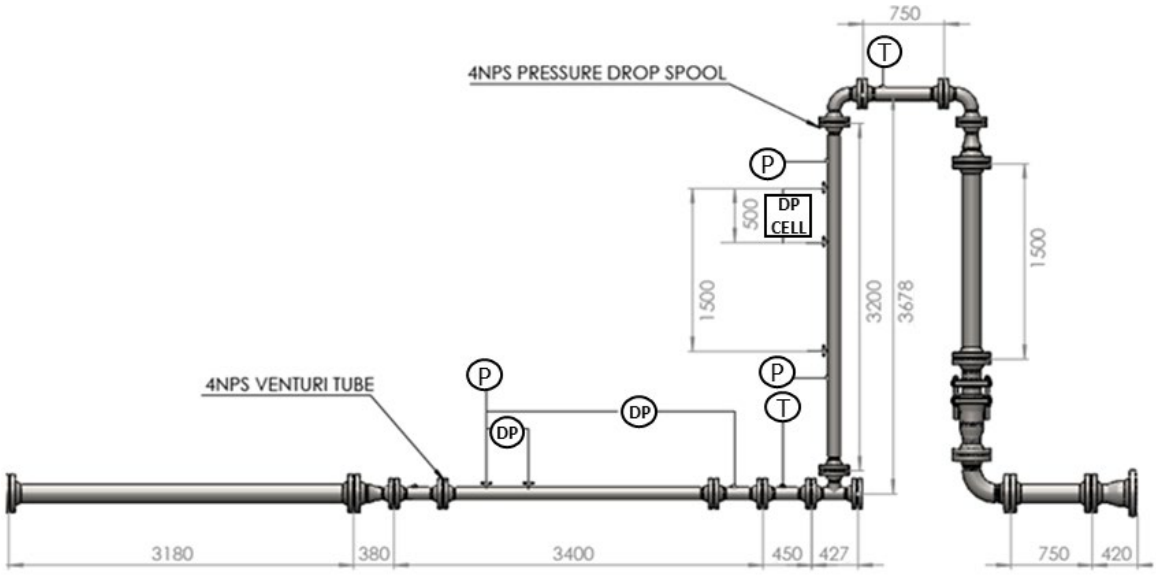

Wet-gas testing is carried out at three different operating pressures (10 bar_g, 18.6 bar_g and 25 bar_g) and three different gas flow rates (450 m^3/h, 250 m^3/h and 112 m^3/h). Pressure and gas flow rate are held constant and the flow rate of liquid is changed to cover a range of void fractions between 0.82 and 0.96 at the vertical test section, and gas mass fractions between approximately 0.17 and 0.72. The dry gas condition for each pressure and gas flowrate is also tested. In total, 55 conditions are tested. A full list of conditions tested with void fraction results is provided in Appendix A.

3.2 Spirax Sarco test description

The steam flow test rig at the Spirax Sarco test centre can provide steam and water flow mixtures with gas mass flow fractions between 0.6 and 1.0 and operating pressure up to 20 bar_g. Individual flow rates of steam and water are controlled using a set of two valves and two pumps, respectively. An additional steam line and heat exchanger is used to raise the water temperature for injection to the steam line in a mixing section. Steam is superheated prior to mixing so that the steam quality is known, and so that water can be injected at the correct pressure and temperature so that the assumption of saturated steam in equilibrium with the water component in the test section can be made. A diagram of the test rig is shown in Figure 3.

An operating pressure of 15 bar_g is used for all test conditions. The operating temperature is approximately that of saturated steam at 15 bar_g, 201 ^oC. Steam flow velocities from 4 to 10 m/s are tested, with gas mass fractions between 0.6 and 0.95 to utilise the full range of conditions available. The test section is carbon steel with inner diameter 2" (52.48 mm). A schematic diagram of the test section is provided in Figure 4. The differential pressure sensor is connected to the two 3/4" flange connections on the vertical line, while other tapping points are used to monitor local temperature and pressure. Differential pressure sensor tapping points are located 500 mm apart as in the first test set at NEL. A full list of conditions tested with void fraction results is provided in Appendix B.

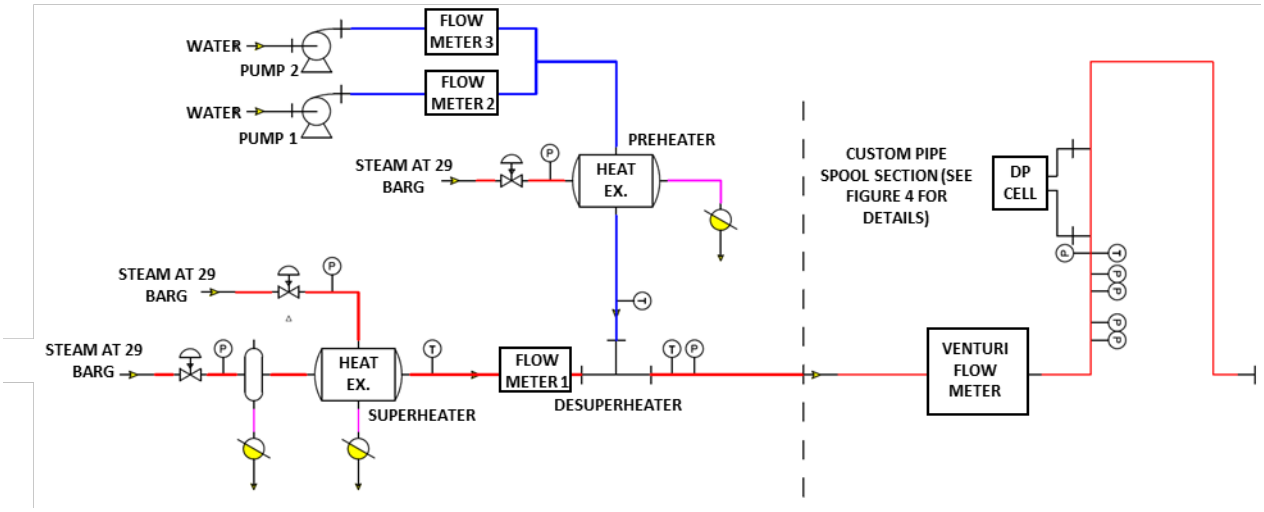

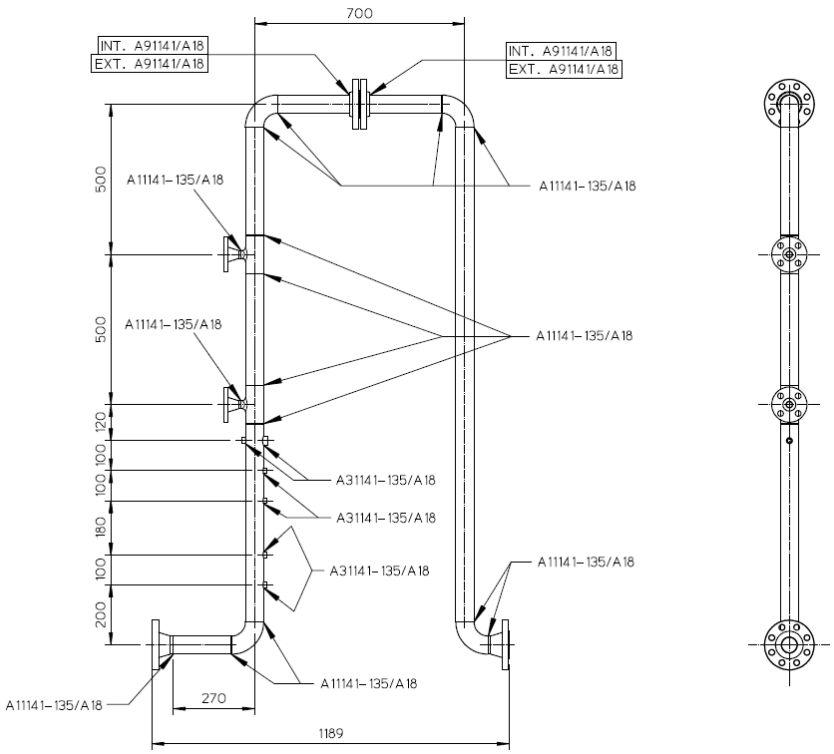

4. Validation of gas void fraction measurements

Both test facilities have measurements of mass and volumetric flow rate for both gas and liquid phase available via single phase flowmeters. In the absence of a direct measurement, the gas void fraction can be estimated using a number of established correlations. This work makes use of a correlation developed for adiabatic two-phase flow in vertical channels by Premoli et al. [18], commonly referred to as the CISE correlation for void fraction. The CISE correlation is commonly used to estimate void fraction in smooth vertical pipe and is used as a benchmark to determine the efficacy of the dP void fraction measurement method. As the dP model assumes a no-slip condition, it is important to validate it against a benchmark which takes this effect into consideration. Of the available correlations for void fraction estimation in two-phase flow, the CISE correlation is most

appropriate for the flow conditions used in these experiments as it is developed using data from turbulent two-phase gas-liquid flow in vertical pipe.

To increase confidence in the estimated void fraction from the CISE correlation, a second method developed by McFarlane [19] which correlates void fraction with the Lockhart-Martinelli parameter [20] is also used. The McFarlane method is valid for flow conditions in which both liquid and gas phases are in the turbulent regime. Void fraction as estimated by the CISE and McFarlane correlations match closely for the tested conditions, and are summarised in Appendix C.

In an ideal situation, the void fraction could be validated using, for example, tomographic methods or quick-closing valves, neither of which were available at either test facility. However, these correlations have been used in previous work to evaluate the quality of experimental data. The work of Lim and Kim [21], Triplett et al. [22] and Idsinga et al. [23] are examples of the CISE correlation being used to compare against experimental data over a wide range of flow conditions. In the absence of a direct void fraction measurement method and with additional confirmation from the McFarlane correlation, this is a valid method to assess the experimental results.

4.1 The CISE correlation

The slip ratio, i.e. the ratio of gas phase velocity to liquid phase velocity (U_g/U_l) in the vertical section must first be calculated. The empirical correlation for slip ratio in two-phase vertical flow developed by Premoli et al. [18] is shown in equation (17).

$$S = 1 + E_1 \left[\left(\frac{y}{1+yE_2} \right) + yE_2 \right]^{0.5} \tag{17}$$

S is the slip ratio, E_1 and E_2 are empirical coefficients and y is calculated from the gas void fraction if homogeneous flow (no slip) is assumed. At homogeneous flow conditions, the void fraction and volume fraction are equal, and can be calculated from the single-phase volumetric flow rates of gas and liquid. Coefficient y is calculated via equation (18).

$$y = \frac{V_{g,hom}}{1-V_{g,hom}} \tag{18}$$

Empirical coefficients E_1 and E_2 are calculated using the liquid-only Reynolds and Weber numbers.

$$Re_{LO} = \frac{DG}{\mu_l} \tag{19}$$

$$We_{LO} = \frac{DG^2}{g\rho_l\sigma} \tag{20}$$

$$E_1 = 1.578 Re_{LO}^{-0.19} \left(\frac{\rho_l}{\rho_g} \right)^{0.22} \tag{21}$$

$$E_1 = 0.0273 We_{LO} Re_{LO}^{-0.51} \left(\frac{\rho_l}{\rho_g} \right)^{-0.08} \tag{22}$$

where G is the total mass flux of the flow, D is the inner pipe diameter and σ is the liquid surface tension. The slip ratio is used to calculate the non-homogeneous gas void fraction as follows:

$$x_g = \frac{m_g}{m_g+m_l} \tag{23}$$

$$\alpha_g = \frac{x_g}{x_g+S(1-x_g)\left(\frac{\rho_g}{\rho_l}\right)} \tag{24}$$

where m_g and m_l are the individual mass flow rates of gas and liquid and x_g is the gas phase mass fraction. The accuracy of the model at each test condition can now be assessed by comparing the gas void fraction from dP measurements with that which is calculated using the CISE correlation. Void fractions calculated from the dP model and CISE correlation, and the deviation of the dP model from the predicted void fraction, are shown in Section 5 for all flow conditions tested.

4.1 The McFarlane correlation

The McFarlane correlation can be used to calculate the void fraction using the Lockhart-Martinelli parameter and takes the form of equation (25). The Lockhart-Martinelli parameter is calculated using the individual volumetric flowrates and densities of liquid and gas, which are available at both test facilities (equation (26)).

$$\alpha_g = 1 - \left[1 + \frac{21}{X} + \frac{1}{X^2}\right]^{-0.5} \quad (25)$$

$$X = \frac{V_l}{V_g}\sqrt{\frac{\rho_l}{\rho_g}} \quad (26)$$

This additional method of calculation is used to double-check the void fraction estimated by the CISE correlation in the absence of a direct void fraction measurement. A comparison between the void fractions predicted by the dP model, the CISE correlation and McFarlane correlation is provided in Appendix C. As the McFarlane correlation and CISE correlation are in close agreement with each other, the CISE correlation can be used with greater confidence as a benchmark to assess the performance of the dP model.

5. Results and Discussion of Void Fraction Measurements

In the figures below the void fraction is plotted both with and without the contribution from frictional effects (equations (15) and (16) respectively). Calculation of the frictional contribution to the void fraction requires knowledge of the flow velocity, which can be estimated using the volumetric flow rates of each individual phase. Reference measurements of single-phase volumetric flow are available at the NEL and Spirax Sarco test centres. This allows the void fraction calculated by the dP model to be compared with the CISE void fraction with and the contribution from frictional effects (equation (15) and equation (16) respectively). Velocity measurements may not always be available in a real process setting but it can be derived via iterative calculation using a Venturi or orifice plate meter, and hence the frictional contribution to pressure drop can be estimated. Void fraction calculated by the dP model with and without frictional component (equations (15) and (16)) are compared with the CISE void fraction (equation (24)) to assess model performance.

5.1. Results from N_2/Water flow system tests, at NEL

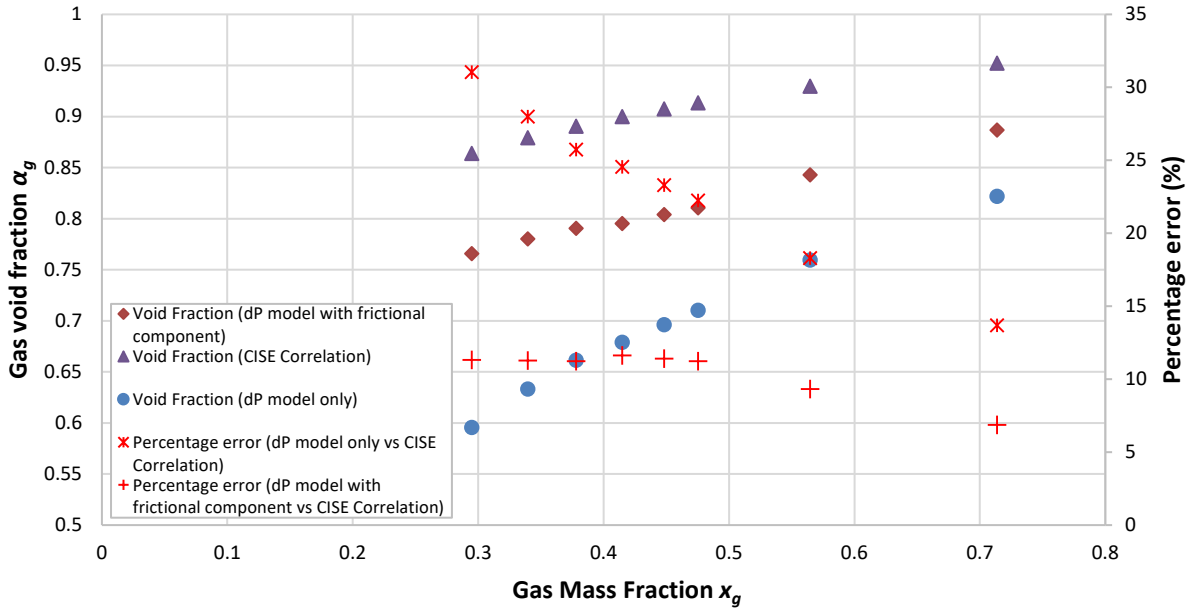

Figure 5. Gas void fraction vs CISE correlation, N_2/Water flow system, 25 bar_g, Gas superficial velocity 16.85 m/s

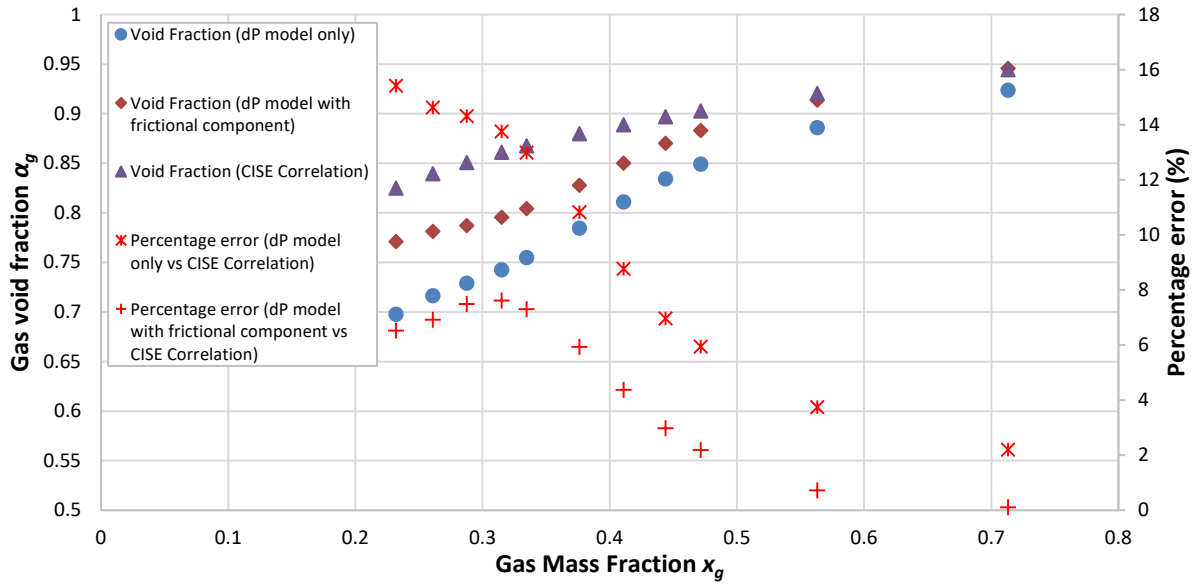

Figure 6. Gas void fraction vs CISE correlation, N_2/Water flow system, 25 bar_g, Gas superficial velocity 9.34 m/s

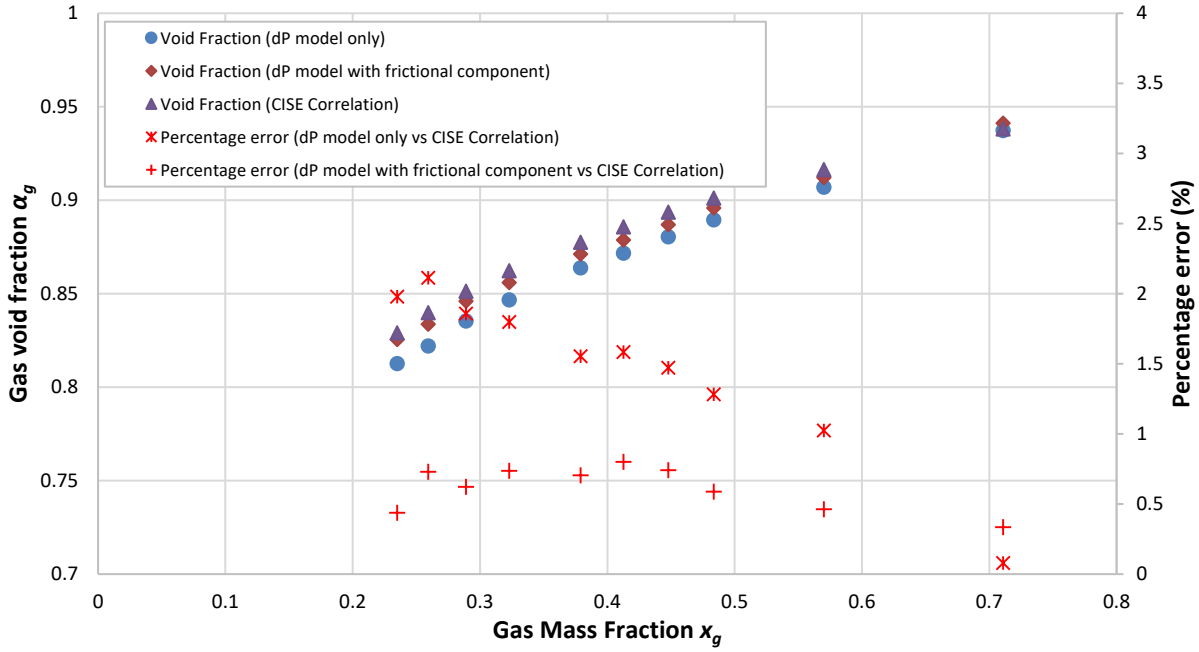

Figure 7. Gas void fraction vs CISE correlation, N_2/Water flow system, 18.6 bar_g, Gas superficial velocity 4.12 m/s

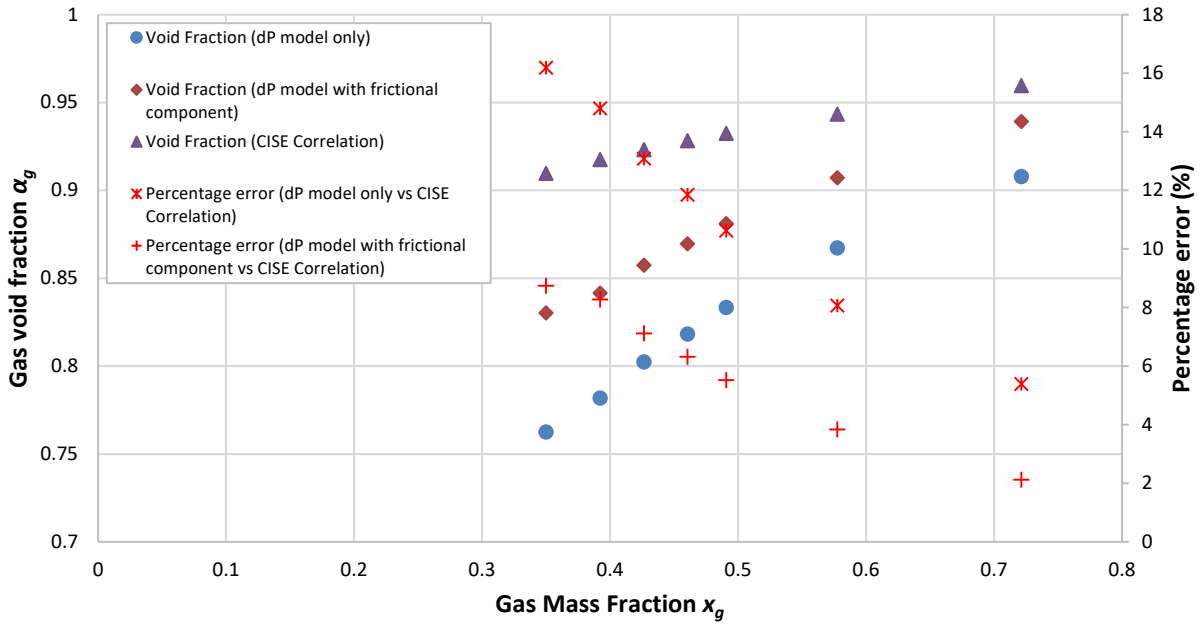

Figure 8. Gas void fraction vs CISE correlation, N_2/Water flow system, 10 bar_g, Gas superficial velocity 16.85 m/s

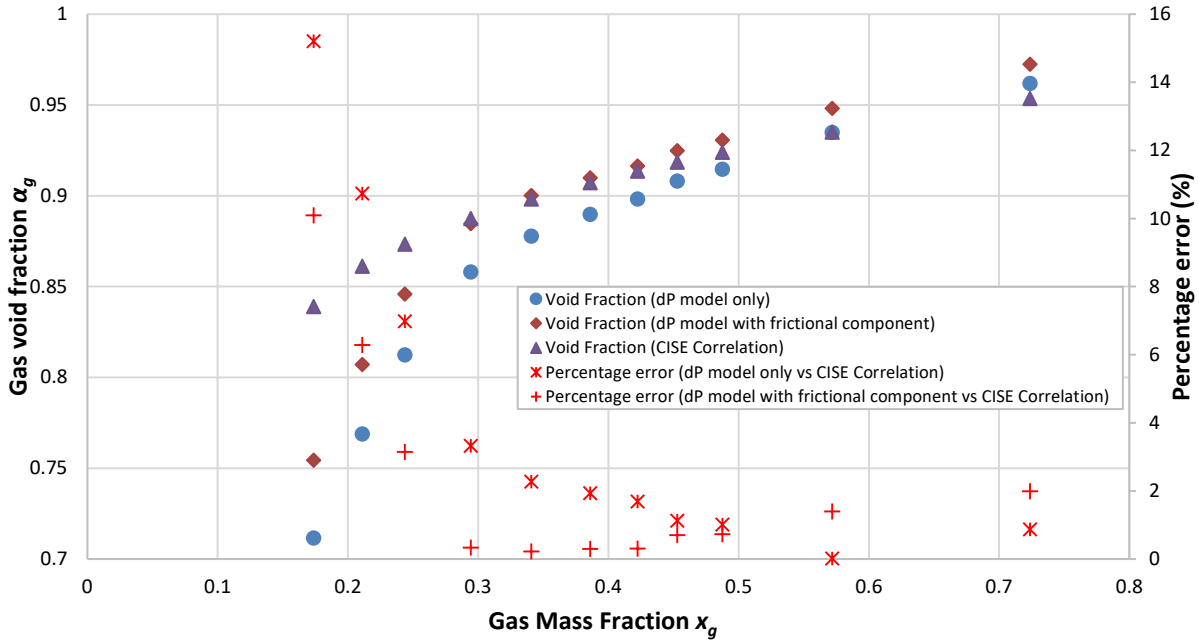

Figure 9. Gas void fraction vs CISE correlation, N_2/Water flow system, 10 bar_g, Gas superficial velocity 9.34 m/s

5.2. Results from Steam/Water flow system tests, Spirax Sarco Test Centre

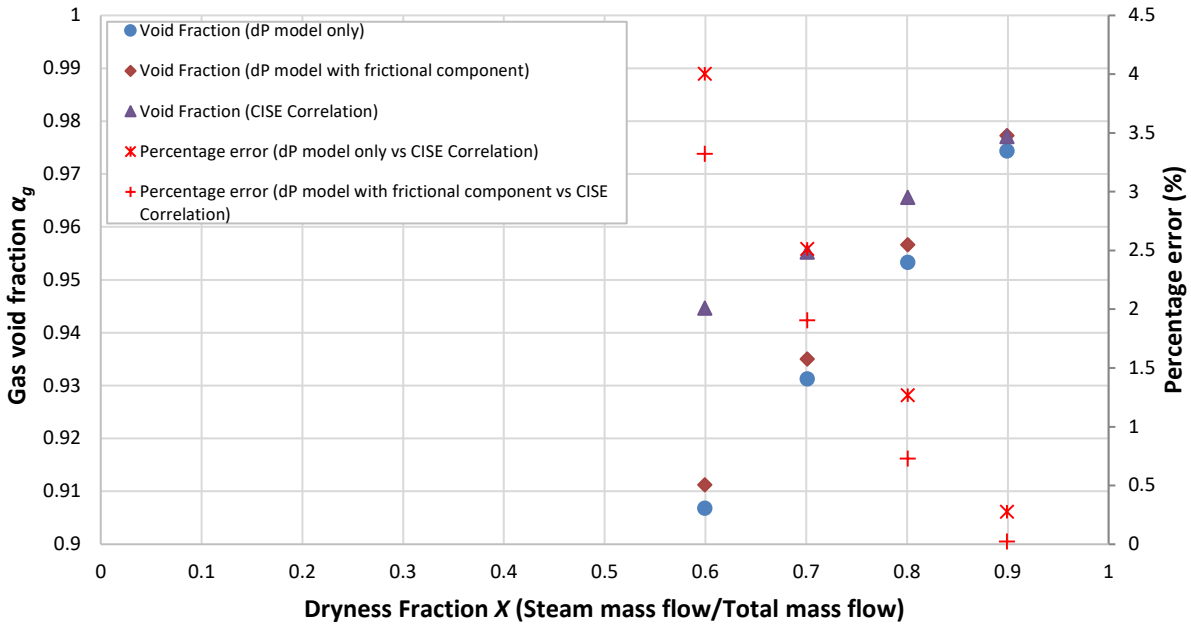

Figure 10. Gas void fraction vs CISE correlation, Steam/Water flow system, 15 bar_g, Gas superficial velocity 4.0 m/s

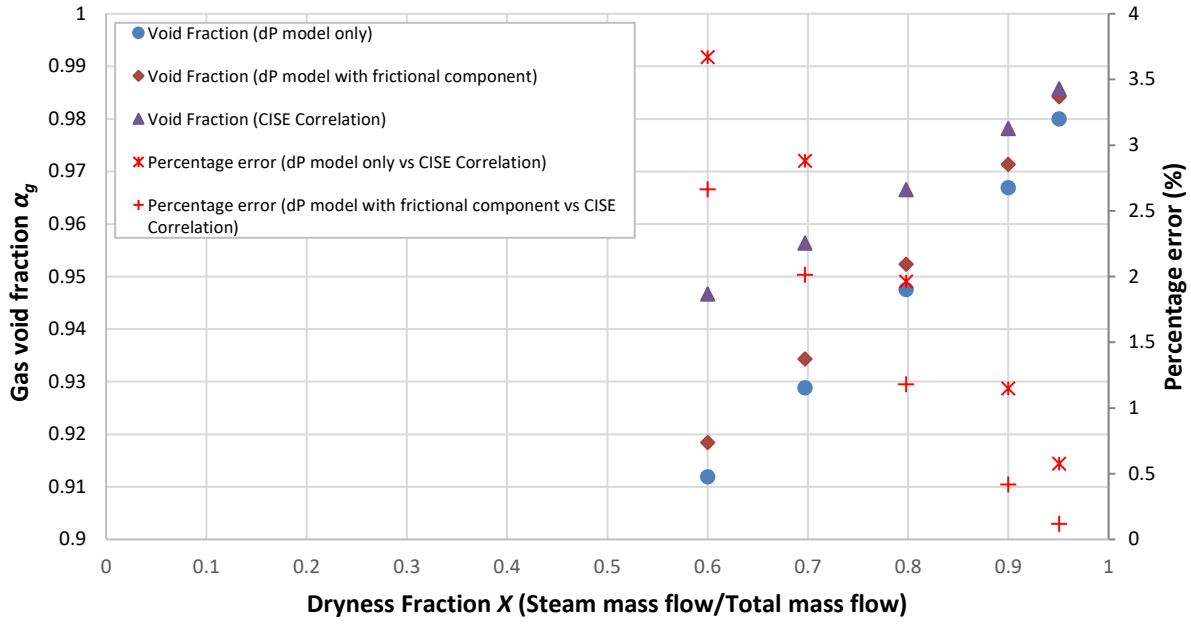

Figure 11. Gas void fraction vs CISE correlation, Steam/Water flow system, 15 bar_g, Gas superficial velocity 5.0 m/s

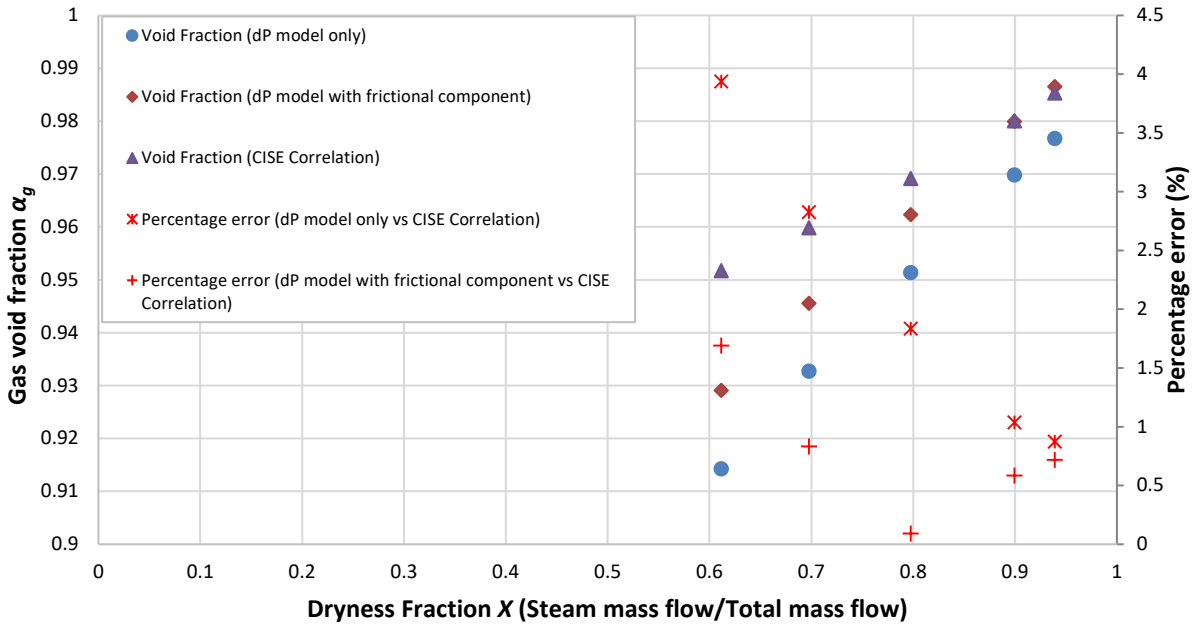

Figure 12. Gas void fraction vs CISE correlation, Steam/Water flow system, 15 bar_g, Gas superficial velocity 8.0 m/s

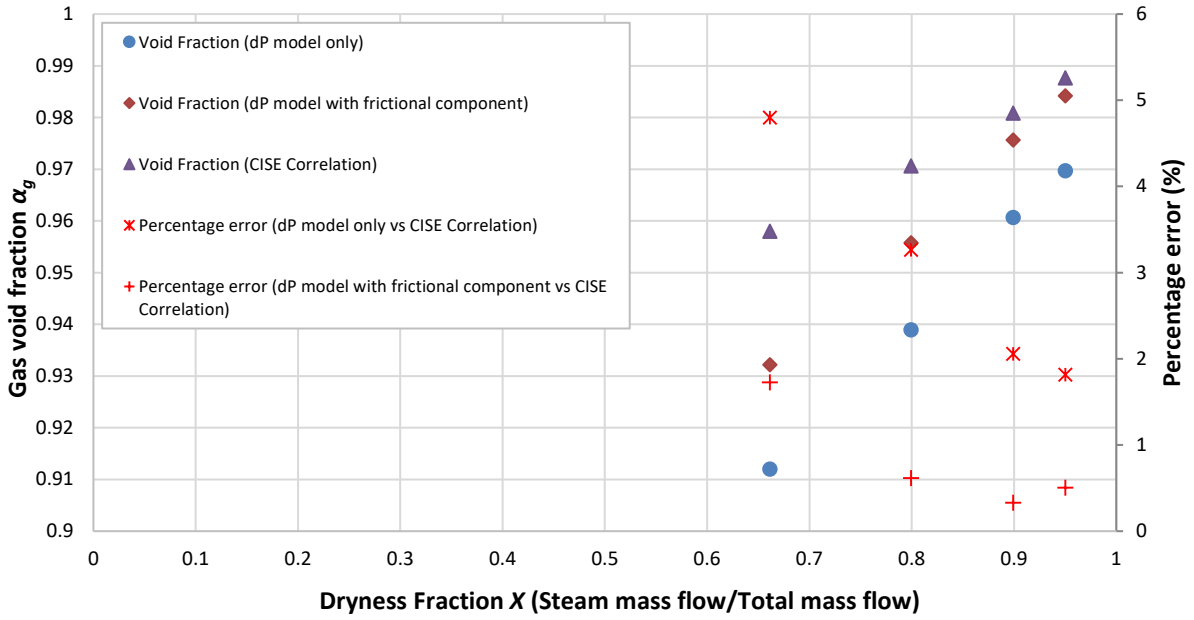

Figure 13. Gas void fraction vs CISE correlation, Steam/Water flow system, 15 bar_g, Gas superficial velocity 10.0 m/s

5.2. Discussion of results

The general trends are similar for all the experimental test conditions. The frictional component of the void fraction is directly proportional to the mixture density and the square of the mean fluid superficial velocity (equation (15)). As a consequence, the model without frictional component performs better at lower velocities and at higher gas mass fractions, as this reduces the overall mixture density. Similarly, lower operating pressure results in a less dense gas and therefore more accurate gas void fraction predictions when using the differential pressure model without the frictional term. This is consistent with the findings of Jia et al. [10] on which this work is based.

Figure 5 shows the void fraction for N_2/water tests at 25 bar_g with gas superficial velocity of 16.85 m/s. The gas void fraction model error without frictional component may be as high as 31%. At this superficial gas velocity, the frictional component is a significant proportion of the total pressure drop, leading to the large difference between the model and CISE correlation. With the frictional component taken into consideration the model performance improves, showing a reduction in maximum error from 31% to 10% compared to the CISE correlation.

For almost all flow conditions on air/water and steam/water systems the results are improved when friction is included (equation (15)) vs when it is approximated to zero (equation (16)). The effects are most significant with high superficial fluid velocity and high pressure, for example Figure 5 shows a maximum improvement of 20% with superficial gas velocity 16.85 m/s, while Figure 7 shows a maximum improvement of 1.6% at 4.12 m/s. This trend is consistent across Figures 5-9.

Tests on steam flow show a considerable improvement in model performance even at gas superficial velocities and mass fractions comparable to the N_2/water tests, with an error below 4.9% for all the tested conditions. These results show that the differential pressure model without frictional term is potentially suitable for steam applications, with high-quality steam and high gas mass fraction as is used in industries such as thermal power generation, food production and pharmaceuticals.

Based on the flow conditions in two experiment campaigns, overall relationship between void fraction and gas mass fraction (flow quality) is non-linear [21][24]. Because the N_2/water test covers a much wider range of gas mass fractions to a minimum of 0.17, the N_2/water flow system displays a more obvious non-linear relationship between gas mass fraction and the gas void fraction. Whereas, all the tests with steam and water have a gas mass fraction greater than 0.6 instead, showing a more linear relationship between gas void fraction and gas mass fraction. For flow systems with high-quality steam, the relationship between void fraction and gas mass fraction can be reasonably approximated with a linear function.

All results show a consistent under-prediction of the differential pressure model. The under-prediction is something which should be addressed in the future development of this method and any future work. This may be a result of under-prediction of the frictional component to the void fraction as a result of inside pipe wall roughness. The true effect of neglecting pipe roughness in future can be investigated by carrying out experiments with pipe of known absolute roughness, recalculating the friction factor C_f using an appropriate expression such as the Swamee-Jain equation, and evaluating these results against those which use the Fanning expression for friction factor (equations (12), (13)). Ideally these results would then be evaluated against wire mesh sensors, tomography, or gamma attenuation measurements.

The flow conditions tested are mapped on the vertical upwards flow diagram of Hewitt and Roberts [25] in Figure 14. All conditions tested on steam/water flows are in the churn region, while the majority of the Nitrogen/water conditions are either churn or annular flow, with a small number in the wispy annular region. Flow regime is estimated for vertical pipe using relative average liquid and gas momentum fluxes and is included to illustrate the range of flow conditions tested in this work.

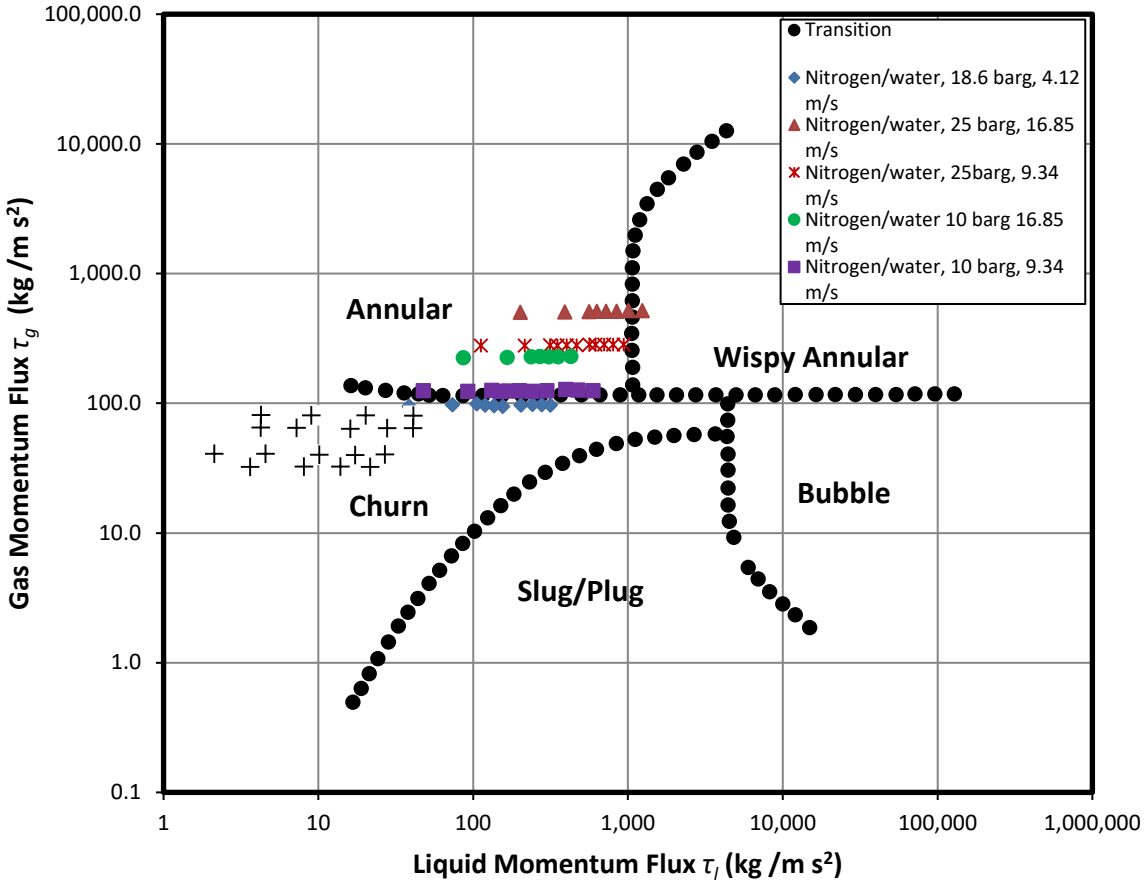

Figure 14. Vertical upward flow map of Hewitt and Roberts [24] with all tested conditions

The dP model assumes homogeneous two-phase flow. In this flow model, the two-phase flow is treated as a hypothetical single phase with uniform velocity over a given cross section, with both phases well dispersed in the other. It would be expected that the model's performance would be most accurate in flow regimes where this is the case, such as under spray or bubble conditions. The two phases are also well dispersed in the annular regime, but the model is able to provide results which are within 5% of the expected value in steam flow tests, which are in the churn flow region. This reflects the complexity of factors affecting the performance of the model.

The performance of the model over each test set initially suggests that it is likely to be most applicable to flow systems which commonly experience churn flow (cf. Figure 7, Figures 10-13), such as in geothermal wells or in nuclear reactor vessel boiling. However, the accuracy of the dP model is affected by many factors related to the frictional contribution to the void fraction, including mean superficial flow velocity, slip ratio, individual and mean two-phase flow densities, all of which will influence the flow regime. To extract the individual effect of each of these factors will require further research.

6. Conclusions

A method of using non-intrusive differential pressure measurement to determine the gas void fraction in vertical pipes with gas mass fractions between 0.17 and 0.95 is presented. The method performs well at relatively low superficial velocity and high gas mass fraction, where the flow regime is closer to churn flow. This method could therefore be employed as a low-cost, non-intrusive monitoring solution for void fraction in high-quality steam flow systems with high gas mass fraction, or in the production of steam from geothermal wells with low velocity. For the nitrogen/water test set with mean flow velocity approximately 4.12 m/s at 18.6 bar_g, the void fraction

measured by the dP model is in agreement with the CISE correlation to within 2.5% of the expected value (Figure 7), as are those conditions above gas mass fraction 0.3 for the test set with mean velocity 9.34 m/s at 10.0 bar_g (Figure 9). For all conditions tested on steam flow systems, the dP model is in agreement with the CISE correlation to within 4.83%. Inclusion of the frictional component improves the performance of the model for almost all conditions tested and significantly in some cases with high pressure, high superficial velocity and low gas mass fraction, reducing the maximum error from 31% to 11.6% (Figure 5).

The findings presented expand on the previous work on the differential pressure method for void fraction measurement by proving its validity at void fractions greater than 0.5. The performance of the model is dependent on several physical parameters which affect the flow regime, including mean flow superficial velocity, mean flow density and viscosity. While there is still scope to improve the model in future research by, for example, more accurate calculation of the frictional contribution to the void fraction, it has been demonstrated to produce void fraction measurements to within 5% of the expected value under certain conditions similar to those of real industrial processes, and has potential for use as a low-cost, non-intrusive flow characterisation method.

7. Glossary of Terms

C_f	Fanning friction factor
D	pipe inner diameter
E_1	CISE correlation coefficient
E_2	CISE correlation coefficient
F_p	pressure loss due to friction
g	acceleration due to gravity
G	mass flux
h	distance between tapping points
m	mass flow rate
P	pressure
Q	volumetric flow rate
Re	Reynolds number
U	Superficial velocity
v	velocity
V	volume fraction
We	Weber number
x	mass fraction
X	Lockhart-Martinelli parameter
y	CISE correlation coefficient

Greek Letters

α	void fraction
ρ	density
μ	dynamic viscosity
τ	momentum flux

Subscripts

g	gas phase
hom	assume homogeneous flow (no slip)
l	liquid phase
LO	consider entire flow as if it were liquid phase only
m	mixture
1, 2	refers to location on test section

Funding

This work was financially supported by Fuji Electric Co., Ltd. Additional contributions were provided in kind by Spirax Sarco Ltd.

8. References

[1] E. Munari, and M. Pinelli, A Review of Wet Gas Flow Rate Measurements by means of Single Phase Meters. Proceedings of ASME Turbomachinery Conference and Exposition GT2018, June 11-15, 2018, Oslo, Norway.

[2] J. Jia, H. Wang and D. Millington, Electrical resistance tomography sensor for highly conductive oil-water two-phase flow measurement, IEEE Sensors Journal. 17 (2017) 8224-8233.

[3] Z. Meng, Z. Huang, B. Wang, H. Ji, H. Li, Y. Yan, Air-water two phase flow measurement using a Venturi meter and an electrical resistance tomography sensor, Flow Measurement and Instrumentation. 21 (2010) 268-276.

[4] A. M. Vasconcelos, R. D. M. Carvalho, O. J. Venturini, F. A. França, The use of the ultrasonic technique for void fraction measurements in air-water bubbly flows. In: Proceedings of the 11th Brazilian Congress of Thermal Sciences and Engineering, Curitiba, Brazil. 2006.
[5] Y. Zheng, Q. Zhang, Simultaneous measurement of gas and solid holdups in multiphase systems using ultrasonic technique. Chemical Engineering Science, 59 (2004) 3505-3514.
[6] F. L. de Oliveira, M.S. Rocha, Experimental facility and void fraction calibration methods for impedance probes. 2013 International Nuclear Atlantic Conference, Recife, Brazil. 2013.
[7] E. Nazemi, G. H. Roshani, S. A. H. Feghhi, S. Setayeshi, E. Eftekhari Zadeh, A. Fatehi, Optimization of a method for identifying the flow regime and measuring void fraction in a broad beam gamma-ray attenuation technique, International Journal of Hydrogen Energy, 41(18) (2016) 7438-7444.
[8] A. A. Kendoush, Z. A. Sarkis, Void fraction measurement by X-ray absorption, Experimental Thermal and Fluid Science. 25 (2002) 615-621.
[9] P. S. L. Yuen, D. A. Meneley, S. Banerjee, Measurement of void fraction by neutron-scattering with portable sources: Effect of the incident energy spectrum. International Journal of Multiphase Flow. 14 (1988) 401-412.
[10] J. Jia, A. Babatunde and M. Wang, Void fraction measurement of gas-liquid two-phase flow from differential pressure, Flow Measurement and Instrumentation. 41 (2015) 75-80.
[11] M. Gui, Z. Liu, B. Liao, T. Wang, Y. Wang, Z. Sui, Q. Bi, J. Wang, Void fraction measurements of steam-water two phase flow in vertical rod bundle: Comparison among different techniques, Experimental Thermal and Fluid Science. 109 (2019) 109881.
[12] F. Hernandez-Alvarado, S. Kleinbart, D. V. Kalaga, S. Banerjee, J. B. Joshi, M. Kawaji, Comparison of void fraction measurements using different techniques in two phase bubble flow reactors, International Journal of Multiphase Flow. 102 (2018) 119-129.
[13] J. Jaeger, C. M. Santos, L. M. Rosa, H. F. Meier, D. Noriler, Experimental and numerical evaluation of slugs in a vertical air-water flow, International Journal of Multiphase Flow. 101 (2018) 152-166.
[14] Y. Deng, N. Jin, Q. Yang, Y. Wang, A differential pressure sensor coupled with conductance sensors to evaluate pressure drop prediction models of gas-water two-phase flow in a vertical small pipe. Sensors. 19 (2019) 2723.
[15] C. F. Colebrook, C. M. White, Experiments with fluid friction in roughened pipes, Proceedings of the Royal Society of London. Series A-Mathematical and Physical Sciences 161 (1937) 367-381.
[16] F. Holland, R. Bragg, Fluid flow for chemical and process engineers, Elsevier, 1995.
[17] A. E. Dukler, W. Moye, R.G. Cleveland, Frictional pressure drop in two-phase flow. Part A: a comparison of existing correlations for pressure loss and holdup, and Part B: an approach through similarity analysis, AIChE J., 10 (1) (1964) 38-51.
[18] A. Premoli, D. Francesco, A. Prima, An empirical correlation for evaluating two-phase mixture density under adiabatic conditions. In: European Two-Phase Flow Group Meeting, Milan, Italy, 1970.
[19] D. R. McFarlane, An analytic study of the transient boiling of sodium in reactor coolant channels. ANL-7222, Argonne National Laboratory, Argonne, USA, 1966.
[20] R. W. Lockhart, R. C. Martinelli, Proposed correlation of data for isothermal two-phase, two component flow in pipes, Chemical Engineering Progress. 45 (1949) 39-48.
[21] T. W. Lim, J. H. Kim, An Experimental Investigation of Pressure Drop in Flow Boiling of Pure Refrigerants and Their Mixture in Horizontal Tube, JSME international journal. Series B, Fluids and thermal engineering, 48 (2005) 92-98.
[22] K. Triplett, S. Ghiaasiaan, S. Abdel-Khalik, A. LeMouel, B. McCord, Gas–liquid two-phase flow in microchannels: part II: void fraction and pressure drop, International Journal of Multiphase Flow, 25 (1999) 395-410.
[23] W. Idsinga, N. Todreas, R. Bowring, An assessment of two-phase pressure drop correlations for steam-water systems, International Journal of Multiphase Flow, 3 (1977) 401-413.
[24] A. J. Ghajar, Void Fraction. In: Two-Phase Gas-Liquid Flow in Pipes with Different Orientations. SpringerBriefs in Applied Sciences and Technology. Springer, Cham. (2020).
[24] G. Hewitt, D. N. Roberts, Studies of two-phase flow patterns by simultaneous X-ray and flash photography, AERE-M-2159, Atomic Energy Research Establishment, Harwell United Kingdom. (1969).

Appendix A. List of N_2/water conditions tested

Table 1. N_2/Water flow system, Pressure approx. 25bar_g, Gas velocity approx 16.85 m/s

Gas mass fraction	N_2 mass flowrate (kg/h)	Water mass flowrate (kg/h)	N_2 superficial velocity (m/s)	Water superficial velocity (m/s)	Operating Pressure (bar_g)	dP Model Void Fraction	CISE Void Fraction	dP model void fraction error (%)
0.295	13831.20	33084.00	16.88	1.241	25.62	0.596	0.864	-31.04
0.340	13842.00	26924.40	16.99	1.010	25.46	0.633	0.879	-27.98
0.378	13701.60	22546.80	16.90	0.846	25.33	0.661	0.890	-25.72
0.415	13640.40	19245.60	16.89	0.722	25.22	0.679	0.900	-24.54
0.448	13669.20	16830.00	16.98	0.631	25.15	0.696	0.908	-23.29
0.475	13593.60	15001.20	16.93	0.563	25.07	0.710	0.913	-22.24
0.565	13525.20	10425.60	16.92	0.391	24.95	0.759	0.929	-18.30
0.714	13438.80	5389.20	16.91	0.202	24.81	0.822	0.952	-13.68

Table 2. N_2/Water flow system, Pressure approx. 25bar_g, Gas velocity approx 9.34 m/s

Gas mass fraction	N_2 mass flowrate (kg/h)	Water mass flowrate (kg/h)	N_2 superficial velocity (m/s)	Water superficial velocity (m/s)	Operating Pressure (bar_g)	dP Model Void Fraction	CISE Void Fraction	dP model void fraction error (%)
0.232	7578.64	25093.81	9.35	0.939	25.22	0.698	0.825	-15.42
0.261	7586.87	21501.47	9.34	0.805	25.17	0.717	0.839	-14.63
0.288	7580.30	18780.56	9.34	0.703	25.13	0.729	0.851	-14.32
0.315	7591.54	16511.75	9.34	0.618	25.10	0.743	0.861	-13.76
0.335	7574.83	15066.76	9.34	0.564	25.06	0.755	0.868	-12.99
0.376	7518.71	12472.59	9.34	0.467	25.01	0.785	0.880	-10.82
0.411	7497.72	10753.35	9.34	0.403	24.97	0.811	0.889	-8.77
0.444	7466.19	9351.89	9.34	0.350	24.95	0.834	0.897	-6.96
0.471	7505.45	8413.53	9.34	0.315	24.92	0.849	0.903	-5.94
0.563	7447.84	5776.85	9.34	0.216	24.87	0.886	0.920	-3.75
0.713	7450.55	2996.41	9.34	0.112	24.81	0.698	0.944	-2.20

Table 3. N_2/Water flow system, Pressure approx. 18.6barg, Gas velocity approx 4.12 m/s

Gas mass fraction	N_2 mass flowrate (kg/h)	Water mass flowrate (kg/h)	N_2 superficial velocity (m/s)	Water superficial velocity (m/s)	Operating Pressure (bar_g)	dP Model Void Fraction	CISE Void Fraction	dP model void fraction error (%)
0.235	2581.20	8402.40	4.19	0.315	19.01	0.813	0.829	-1.98
0.259	2595.60	7412.40	4.21	0.278	19.00	0.822	0.840	-2.11
0.289	2617.20	6440.40	4.25	0.242	18.98	0.835	0.851	-1.86
0.323	2588.40	5428.80	4.21	0.204	18.96	0.847	0.862	-1.80
0.379	2534.40	4150.80	4.13	0.156	18.94	0.864	0.878	-1.56
0.413	2556.00	3636.00	4.17	0.136	18.91	0.872	0.886	-1.58
0.448	2588.40	3189.60	4.23	0.120	18.90	0.881	0.894	-1.47
0.484	2642.40	2822.40	4.32	0.106	18.88	0.890	0.901	-1.28
0.570	2602.80	1962.00	4.25	0.074	18.88	0.907	0.916	-1.02
0.711	2530.80	1029.60	4.16	0.039	18.73	0.937	0.938	-0.08

Table 4. N_2/Water flow system, Pressure approx. 10.5 bar_g, Gas velocity approx 16.85 m/s

Gas mass fraction	N_2 mass flowrate (kg/h)	Water mass flowrate (kg/h)	N_2 superficial velocity (m/s)	Water superficial velocity (m/s)	Operating Pressure (bar_g)	dP Model Void Fraction	CISE Void Fraction	dP model void fraction error (%)
0.350	6134.40	11397.60	16.77	0.428	10.58	0.763	0.910	-16.19
0.392	6105.60	9460.80	16.75	0.355	10.56	0.782	0.918	-14.80
0.427	6112.80	8215.20	16.80	0.308	10.59	0.802	0.923	-13.08
0.461	6130.80	7182.00	16.89	0.269	10.55	0.818	0.928	-11.85
0.491	6098.40	6328.80	16.83	0.237	10.54	0.833	0.933	-10.63
0.578	6040.80	4417.20	16.76	0.166	10.51	0.867	0.943	-8.07
0.721	5986.80	2311.20	16.71	0.087	10.49	0.908	0.960	-5.39

Table 5. N_2/Water flow system, Pressure approx. 10.5 bar_g, Gas velocity approx 9.34 m/s

Gas mass fraction	N_2 mass flowrate (kg/h)	Water mass flowrate (kg/h)	N_2 superficial velocity (m/s)	Water superficial Velocity (m/s)	Operating Pressure (bar_g)	dP Model Void Fraction	CISE Void Fraction	dP model void fraction error (%)
0.174	3330.00	15829.20	8.59	0.594	10.53	0.711	0.839	-15.20
0.211	3384.00	12654.00	9.34	0.475	10.61	0.769	0.861	-10.73
0.244	3409.20	10573.20	9.43	0.397	10.61	0.812	0.873	-6.98
0.294	3333.60	7992.00	9.25	0.300	10.59	0.858	0.887	-3.32
0.341	3297.60	6375.60	9.17	0.239	10.58	0.878	0.898	-2.27
0.386	3337.20	5310.00	9.29	0.199	10.57	0.890	0.907	-1.93
0.422	3322.80	4543.20	9.26	0.170	10.56	0.898	0.914	-1.69
0.453	3294.00	3978.00	9.19	0.149	10.55	0.908	0.918	-1.12
0.487	3355.20	3528.00	9.38	0.132	10.55	0.915	0.924	-1.01
0.572	3294.00	2466.00	9.22	0.093	10.54	0.935	0.935	-0.02
0.724	3330.00	1270.80	9.33	0.048	10.53	0.962	0.954	0.87

Appendix B. List of steam/water conditions tested

Table 6. Steam/Water flow system, all flow conditions

Gas mass fraction	Steam mass flowrate (kg/h)	Water mass flowrate (kg/h)	Steam superficial velocity (m/s)	Liquid superficial velocity (m/s)	Operating Pressure (bar_g)	dP Model Void Fraction	CISE Void Fraction	dP model void fraction error (%)
0.599	251.17	167.98	3.99	0.0250	14.99	0.907	0.945	-4.003
0.701	253.23	108.09	4.02	0.0161	15.00	0.931	0.955	-2.512
0.801	252.74	62.94	4.01	0.0094	15.00	0.953	0.966	-1.269
0.899	251.94	28.24	4.00	0.0042	15.02	0.974	0.977	-0.276
0.600	314.58	209.70	4.99	0.0312	15.01	0.912	0.947	-3.672
0.697	310.12	134.62	4.92	0.0200	15.00	0.929	0.956	-2.881
0.798	312.07	79.03	4.95	0.0118	15.01	0.948	0.967	-1.964
0.900	317.77	35.39	5.05	0.0053	14.99	0.967	0.978	-1.149
0.951	318.17	16.52	5.05	0.0025	14.99	0.980	0.986	-0.577
0.611	502.05	319.12	7.98	0.0475	14.98	0.914	0.952	-3.937
0.698	499.85	216.73	7.94	0.0322	14.99	0.933	0.960	-2.827
0.797	494.20	125.53	7.83	0.0187	15.03	0.951	0.969	-1.836
0.899	502.38	56.18	7.99	0.0084	14.98	0.970	0.980	-1.038
0.939	507.93	33.01	8.06	0.0049	15.00	0.977	0.985	-0.873
0.661	623.38	319.32	9.90	0.0475	15.00	0.912	0.958	-4.802

0.799	627.15	157.55	9.96	0.0234	14.99	0.939	0.971	-3.266
0.899	627.06	70.21	9.96	0.0104	14.99	0.961	0.981	-2.059
0.950	634.01	33.21	10.07	0.0049	14.99	0.970	0.988	-1.818

Appendix C. Comparison between CISE and McFarlane void fractions

Table 7. N_2/Water flow system, Pressure approx. 25bar$_g$, Gas velocity approx 16.85 m/s

Gas mass fraction	Steam mass flowrate (kg/h)	Water mass flowrate (kg/h)	Void fraction with static head component only (dP model)	Void fraction with frictional component (dP model)	CISE void fraction	McFarlane void fraction
0.295	13831.20	33084.00	0.596	0.765	0.864	0.867
0.340	13842.00	26924.40	0.633	0.784	0.879	0.882
0.378	13701.60	22546.80	0.661	0.790	0.890	0.892
0.415	13640.40	19245.60	0.679	0.795	0.900	0.902
0.448	13669.20	16830.00	0.696	0.803	0.908	0.909
0.475	13593.60	15001.20	0.710	0.810	0.913	0.915
0.565	13525.20	10425.60	0.759	0.840	0.929	0.932
0.714	13438.80	5389.20	0.822	0.886	0.952	0.956

Table 8. N_2/Water flow system, Pressure approx. 25bar$_g$, Gas velocity approx 9.34 m/s

Gas mass fraction	Steam mass flowrate (kg/h)	Water mass flowrate (kg/h)	Void fraction with static head component only (dP model)	Void fraction with frictional component (dP model)	CISE void fraction	McFarlane void fraction
0.232	7578.64	25093.81	0.698	0.771	0.825	0.843
0.261	7586.87	21501.47	0.717	0.781	0.839	0.855
0.288	7580.30	18780.56	0.729	0.787	0.851	0.865
0.315	7591.54	16511.75	0.743	0.795	0.861	0.875
0.335	7574.83	15066.76	0.755	0.804	0.868	0.881
0.376	7518.71	12472.59	0.785	0.828	0.880	0.892
0.411	7497.72	10753.35	0.811	0.850	0.889	0.901
0.444	7466.19	9351.89	0.834	0.870	0.897	0.908
0.471	7505.45	8413.53	0.849	0.883	0.903	0.914
0.563	7447.84	5776.85	0.886	0.914	0.920	0.932
0.713	7450.55	2996.41	0.698	0.945	0.944	0.956

Table 9. N_2/Water flow system, Pressure approx. 18.6bar$_g$, Gas velocity approx 4.12 m/s

Gas mass fraction	Steam mass flowrate (kg/h)	Water mass flowrate (kg/h)	Void fraction with static head component only (dP model)	Void fraction with frictional component (dP model)	CISE void fraction	McFarlane void fraction
0.235	2581.20	8402.40	0.813	0.825	0.829	0.855
0.259	2595.60	7412.40	0.822	0.834	0.840	0.865
0.289	2617.20	6440.40	0.835	0.846	0.851	0.875
0.323	2588.40	5428.80	0.847	0.856	0.862	0.886
0.379	2534.40	4150.80	0.864	0.871	0.878	0.901
0.413	2556.00	3636.00	0.872	0.879	0.886	0.909
0.448	2588.40	3189.60	0.881	0.887	0.894	0.916
0.484	2642.40	2822.40	0.890	0.896	0.901	0.923
0.570	2602.80	1962.00	0.907	0.912	0.916	0.938
0.711	2530.80	1029.60	0.937	0.941	0.938	0.959

Table 10. N_2/Water flow system, Pressure approx. 10.5 bar_g, Gas velocity approx 16.85 m/s

Gas mass fraction	Steam mass flowrate (kg/h)	Water mass flowrate (kg/h)	Void fraction with static head component only (dP model)	Void fraction with frictional component (dP model)	CISE void fraction	McFarlane void fraction
0.350	6134.40	11397.60	0.763	0.858	0.910	0.921
0.392	6105.60	9460.80	0.782	0.830	0.918	0.904
0.427	6112.80	8215.20	0.802	0.842	0.923	0.914
0.461	6130.80	7182.00	0.818	0.870	0.928	0.928
0.491	6098.40	6328.80	0.833	0.881	0.933	0.933
0.578	6040.80	4417.20	0.867	0.907	0.943	0.947
0.721	5986.80	2311.20	0.908	0.939	0.960	0.967

Table 11. N_2/Water flow system, Pressure approx. 10.5 bar_g, Gas velocity approx 9.34 m/s

Gas mass fraction	Steam mass flowrate (kg/h)	Water mass flowrate (kg/h)	Void fraction with static head component only (dP model)	Void fraction with frictional component (dP model)	CISE void fraction	McFarlane void fraction
0.174	3330.00	15829.20	0.711	0.754	0.839	0.832
0.211	3384.00	12654.00	0.769	0.807	0.861	0.859
0.244	3409.20	10573.20	0.812	0.846	0.873	0.873
0.294	3333.60	7992.00	0.858	0.885	0.887	0.890
0.341	3297.60	6375.60	0.878	0.900	0.898	0.903
0.386	3337.20	5310.00	0.890	0.910	0.907	0.914
0.422	3322.80	4543.20	0.898	0.916	0.914	0.921
0.453	3294.00	3978.00	0.908	0.925	0.918	0.927
0.487	3355.20	3528.00	0.915	0.931	0.924	0.933
0.572	3294.00	2466.00	0.935	0.948	0.935	0.947
0.724	3330.00	1270.80	0.962	0.972	0.954	0.967

Table 12. Steam/Water flow system, All flow conditions

Gas mass fraction	Steam mass flowrate (kg/h)	Water mass flowrate (kg/h)	Void fraction with static head component only (dP model)	Void fraction with frictional component (dP model)	CISE void fraction	McFarlane void fraction
0.599	251.17	167.98	0.907	0.911	0.945	0.958
0.701	253.23	108.09	0.931	0.935	0.955	0.970
0.801	252.74	62.94	0.953	0.957	0.966	0.980
0.899	251.94	28.24	0.974	0.977	0.977	0.990
0.600	314.58	209.70	0.912	0.918	0.947	0.958
0.697	310.12	134.62	0.929	0.934	0.956	0.969
0.798	312.07	79.03	0.948	0.952	0.967	0.980
0.900	317.77	35.39	0.967	0.971	0.978	0.990
0.951	318.17	16.52	0.980	0.984	0.986	0.995
0.611	502.05	319.12	0.914	0.929	0.952	0.959
0.698	499.85	216.73	0.933	0.945	0.960	0.969
0.797	494.20	125.53	0.951	0.962	0.969	0.980
0.899	502.38	56.18	0.970	0.979	0.980	0.990
0.939	507.93	33.01	0.977	0.986	0.985	0.994
0.661	623.38	319.32	0.912	0.932	0.958	0.965
0.799	627.15	157.55	0.939	0.955	0.971	0.980

0.899	627.06	70.21	0.961	0.975	0.981	0.990
0.950	634.01	33.21	0.970	0.984	0.988	0.995